BBA - Biomembranes 1865 (2023) 184173

Contents lists available at ScienceDirect

BBA - Biomembranes

journal homepage: www.elsevier.com/locate/bbamem

Multiplexed imaging for probing RAS-RAF interactions in living cells

Mohammad Ahmad [a], Liviu Movileanu [a,b,c,*]

[a] Department of Physics, Syracuse University, 201 Physics Building, Syracuse, New York 13244-1130, USA
[b] Department of Biomedical and Chemical Engineering, Syracuse University, 329 Link Hall, Syracuse, NY 13244, USA
[c] The BioInspired Institute, Syracuse University, Syracuse, NY 13244, USA

ARTICLE INFO

Keywords:
Protein-protein interactions
Cell signaling
Binding affinity
Intracellular measurements
Protein engineering
GTPase
EGFR
Multicolor microscopy

ABSTRACT

GTP-bound RAS interacts with its protein effectors in response to extracellular stimuli, leading to chemical inputs for downstream pathways. Significant progress has been made in measuring these reversible protein-protein interactions (PPIs) in various cell-free environments. Yet, acquiring high sensitivity in heterogeneous solutions remains challenging. Here, using an intermolecular fluorescence resonance energy transfer (FRET) biosensing approach, we develop a method to visualize and localize HRAS-CRAF interactions in living cells. We demonstrate that the EGFR activation and the HRAS-CRAF complex formation can be concurrently probed in a single cell. This biosensing strategy discriminates EGF-stimulated HRAS-CRAF interactions at the cell and organelle membranes. In addition, we provide quantitative FRET measurements for assessing these transient PPIs in a cell-free environment. Finally, we prove the utility of this approach by showing that an EGFR-binding compound is a potent inhibitor of HRAS-CRAF interactions. The outcomes of this work form a fundamental basis for further explorations of the spatiotemporal dynamics of various signaling networks.

1. Introduction

Mitogen-activated and extracellular signal-regulated protein kinase (MEK/ERK) signaling is critical for cell growth, differentiation, and proliferation [1]. RAS proteins are small monomeric guanosine triphosphatases (GTPases) that participate in this pathway [2]. They function as molecular switches between an active GTP-bound state and an inactive GDP-bound state, mediating the transmission of external signals to downstream effectors. Because mutations of upstream receptors, such as the epidermal growth factor receptor (EGFR) and RAS proteins, are frequently encountered in numerous cancers, this signaling network is a crucial therapeutic target [3,4]. For example, selective and specific mutations in RAS proteins lead to subsequent constitutive activation of the MEK/ERK signaling, a driver in oncogenesis [5–7]. EGFR signaling is initiated by binding the epidermal growth factor (EGF) ligand to EGFR (Fig. 1), leading to receptor dimerization and subsequent activation of intracellular signaling cascades. Once EGF induces EGFR dimerization, autophosphorylation occurs, attracting Grb2/SOS. This process stimulates HRAS on the cell membrane, and the nucleotide exchange factor replaces GDP with GTP. Activated RAS transmits the signal downstream *via* the RAF/MEK/ERK pathway into the nucleus, leading to transcriptional regulation of target genes that promote cell proliferation and survival. The proper membrane localization and interaction of RAS with its downstream effectors, including RAF, are facilitated by farnesylation and palmitoylation. These two processes employ lipid modifications that occur on the C-terminal cysteine residue of RAS and play a central role in the proper localization and stability of these proteins at the cell membrane. Therefore, farnesylation and palmitoylation are significant in initiating and propagating the EGFR signaling pathway.

Among the three isoforms, HRAS has been studied as representative of the specific structural fingerprint at the interface of RAS with its regulatory proteins and effectors [5]. Activated RAS switchers associate with their RAF protein effectors for further signaling transmission *via* RAS/RAF/MEK/ERK [8–10]. There are three RAF isoforms, BRAF, CRAF, and ARAF. CRAF is essential for the input transmission of HRAS-activated signaling in mammalian cells [11]. Therefore, it is imperative to develop tractable, versatile, and sensitive approaches that can be used to probe, localize, and evaluate these transient protein-protein interactions (PPIs) [12–14]. In addition, it is desirable to explore their spatiotemporal dynamics and coordination with other events of a specific signaling pathway.

Quantifications of the kinetics and affinity of RAS-RAF interactions were previously performed using various prevailing techniques for

* Corresponding author at: Department of Physics, Syracuse University, 201 Physics Building, Syracuse, NY 13244-1130, USA.
E-mail address: lmovilea@syr.edu (L. Movileanu).

https://doi.org/10.1016/j.bbamem.2023.184173
Received 16 January 2023; Received in revised form 18 April 2023; Accepted 8 May 2023
Available online 19 May 2023

characterizing transient PPIs in homogeneous solutions, such as isothermal calorimetry (ITC) [15], fluorescence microscopy [16], biolayer interferometry (BLI) [6], surface plasmon resonance (SPR) [17], and fluorescence polarization (FP) spectroscopy [18]. Furthermore, a bioluminescence resonance energy transfer (BRET)-based imaging method has been developed to monitor binding preferences for RAS with various RAF family members in living cells [19]. Detections of small GTPase activity and RAS-effector interactions in living cells have also been conducted using intramolecular fluorescence resonance energy transfer (FRET) sensors [20,21]. The dynamic range is usually lower in intramolecular FRET because the binding domains and the FRET pair are fully interconnected. However, a significant advantage of intermolecular FRET is that its dynamic range is significantly broader [22,23]. In intermolecular FRET, the donor and acceptor fluorophores are attached to two separate interacting proteins [24–26]. In general, the cyan (CFP) - yellow (YFP) fluorescent protein pair is the most routinely utilized couple of protein fluorophores for *in vitro* and *in vivo* FRET assays [27–29], including those for reversible PPIs [30]. mVenus is a monomeric yellow fluorescent protein (mYFP) with high photostability and brightness [31,32]. Furthermore, mScarlet-I is the least phototoxic fluorophore in HeLa cells. It is also the brightest fluorophore among all monomeric red fluorescent proteins (mRFPs) [33].

Here, we propose acceptor-photobleaching (abFRET) and sensitized-emission (seFRET) FRET approaches to detect and quantify HRAS-CRAF interactions at high spatiotemporal resolution using a yellow-red pair. To enhance our understanding of HRAS-CRAF dynamics in living cells, we have generated different variants of HRAS and CRAF. We then extensively characterized their interactions in living cells and a cell-free environment. In addition, we demonstrated that this yellow-red fluorescent protein pair is highly compatible with a cyan fluorescent protein, thereby achieving spatiotemporal dissection of targeted activity under dynamic control of cellular functions. Using the HRAS- and CRAF-labeled proteins, along with an engineered EGFR biosensor, we spatially identified specific activity profiles of EGFR and subsequent HRAS-CRAF interactions in a single cell. This development proved the utility of our approach for the real-time monitoring of the EGFR signaling pathway at the cellular and sub-cellular levels.

2. Results and discussion

2.1. Development and characterization of a yellow-red pair

To evaluate this pair of fluorophores, we created pmScarlet-I-PEP-mVenus and pmScarlet-I-T2A-mVenus fusion proteins as positive- and negative-FRET controls, respectively (Materials and Methods). These constructs include two short peptides, PEP and T2A, whose sequences are SGSGLRSSDPPVAT and EGRGSLLTCGDVEENPGP (Supplementary Fig. S1, Fig. S2a, Table S1), respectively [34]. T2A has a self-cleaving peptide sequence that enables the expression of multiple proteins from a single mRNA transcript. This peptide sequence functions by inducing a "ribosomal skip" event during the translation, in which the ribosome pauses and resumes the translation downstream of the T2A sequence. This process releases the nascent polypeptide chain containing the upstream protein of interest while the downstream protein is simultaneously synthesized. Following the expression of positive and negative FRET controls, lysates of HeLa cells were subjected to an immunoblot analysis, which confirmed their molecular weight (Supplementary Fig. S2b). The transfected cells were then characterized by lambda-scanning mode (Materials and Methods). Fluorescence images and emission spectrum were recorded by exciting the sample with the donor excitation for both positive and negative FRET controls. We observed the acceptor emission peak at the RFP channel in positive FRET control-expressing cells by the excitation of the donor (Supplementary Fig. S2c). This finding confirms the seFRET signal of the mVenus - mScarlet-I pair. However, very low emission of mScarlet-I was noted in the negative FRET control-expressing cells (Supplementary Fig. S2d). The immunoblot analysis confirmed the expression and size of mVenus, mVenus-HRAS, mVenus-HRAS-DN, RBD-mScarlet-I, mScarlet-I, and CRAF-mScarlet-I (Supplementary Fig. S3a). Here, RBD is the RAS-binding domain of CRAF [35], which mainly interacts with HRAS

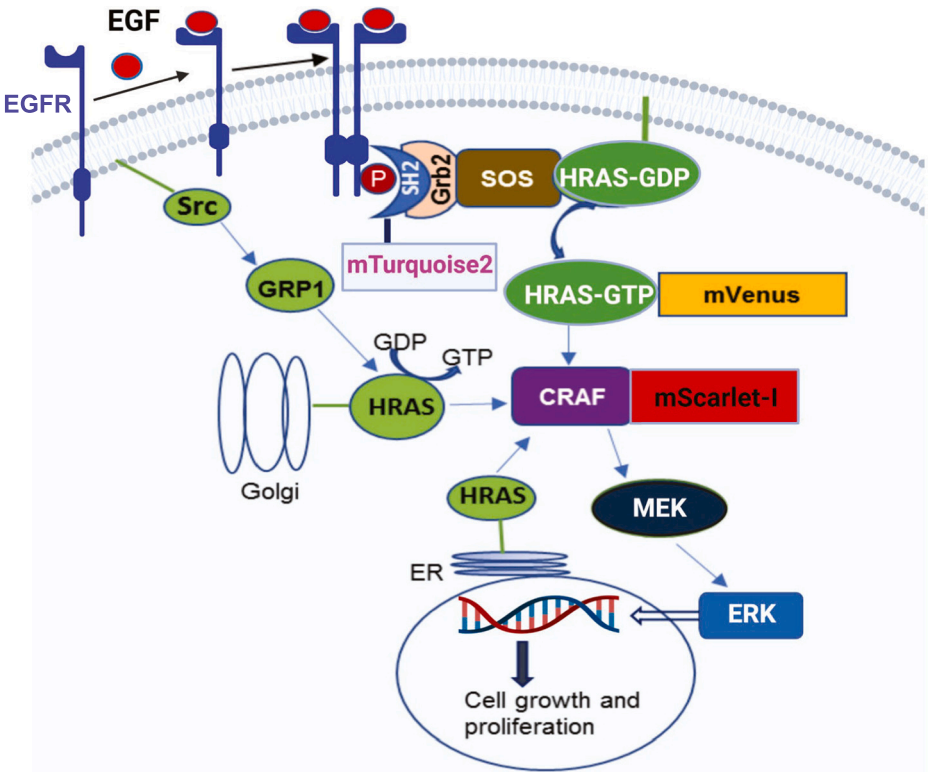

Fig. 1. MEK-ERK signaling pathway involving HRAS-CRAF interactions. Signal propagation through HRAS compartmentalizes signal transduction both at the cell surface and through differential interactions with endomembranes. Epidermal growth factor (EGF)-induced dimerization of epidermal growth factor receptor (EGFR) activates HRAS on the cell membrane by attracting Grb2/SOS and transmitting the signal *via* HRAS/CRAF/MEK/ERK. The signal flows by these components into the nucleus, which leads to the cell proliferation in response to external stimuli. In addition, Src is also recruited to activated EGFRs at the cell membrane. The activation of Src amplifies the intracellular calcium, leading to the activation of GRP1 protein. Then, GRP1 translocates to Golgi, stimulating HRAS.

[36]. HRAS-DN, an S17N HRAS mutant, is a dominant-negative HRAS variant exhibiting weak interactions with CRAF [16]. Upon expressing mVenus-HRAS in HeLa cells, we observed that HRAS was localized at the cell membrane and membranes of Golgi and endoplasmic reticulum (ER) (Supplementary Fig. S3b; Movie S1a), similar to the endogenous HRAS [37]. We found that the distributions of HRAS at the cell and Golgi membranes were more heterogeneous than at the ER endomembrane (Supplementary Fig. S3c). Next, we validated the organelle localization of HRAS using Golgi and ER markers. Co-expression analysis showed a significant signal overlap between mVenus-HRAS and mScarlet-I-giantin (Golgi) as well as between mVenus-HRAS and mScarlet-I-KDEL (ER) (Supplementary Fig. S4a-b). Giantin is a widely expressed Golgi-conserved membrane protein frequently used as a biomarker for Golgi visualization [38]. Biochemical evidence suggests giantin's role in tethering endosomes in intracellular signaling [39]. CRAF was localized into the cytosol of HeLa cells (Supplementary Fig. S4c1). In addition to RBD, the cysteine-rich domain (CRD) of CRAF (RBDCRD) also shows interactions with HRAS [36]. However, the interaction pattern of this domain was not characterized in living cells. The RBD and RBDCRD do not have cytosol-specific localization, so they diffused into the nucleus (Supplementary Fig. S4c2-c3). Hence, we genetically fused a nuclear export signal (NES) peptide to RBD. The NES was an extension to the C-terminus of mScarlet-I to avoid any interference with HRAS-RBD interactions. Therefore, we localized the RBD-mScarlet-I_NES within the cytosol (Supplementary Fig. S4c4; Supplementary Movie S1b).

2.2. Probing HRAS-CRAF interactions in living cells using seFRET

For most FRET pairs, the spectral overlap necessitated for the FRET output is also a cause of FRET signal contamination. On the one hand, the acceptor is directly excited by the donor excitation, also named the acceptor spectral bleed-through (ASBT). On the other hand, some donor emission overlaps with the acceptor emission, also called the donor spectral bleed-through (DSBT). We experimentally determined these factors by examining HeLa cells expressing either the donor or the acceptor (Materials and Methods; Supplementary Fig. S5, Table S2). The NFRET is the normalized seFRET, which was obtained by subtracting ASBT and DSBT from the raw FRET signal. HeLa cells were transfected with positive- and negative-FRET control plasmids and subjected to imaging in living cells. Initially, three groups of cells were selected, expressing different concentrations of FRET pairs, and NFRET values were calculated (Materials and Methods; Supplementary Fig. S6). NFRET values did not change if the ratio of donor emission to acceptor emission was maintained. Next, NFRET values of positive FRET control-expressing cells showed a high FRET efficiency (Fig. 2a), likely due to the proximity of the donor to the acceptor. In contrast, negative FRET control-expressing cells did not exhibit any significant NFRET signal (Fig. 2b). We then interrogated HRAS-CRAF interactions in the presence of EGF, which stimulates the MEK/ERK pathway [40]. The seFRET analysis of the co-expressed mVenus-HRAS-DN and RBD-mScarlet-I confirmed weak interactions (Fig. 2c). The Q61L mutation of HRAS, also named HRAS-CA, produces constitutive activity of this GTPase [5,41,42]. HRAS-CA is associated with several types of cancer [43]. Images of HeLa cells co-expressing mVenus-HRAS-CA + RBD-mScarlet-I_NES were recorded and analyzed at various channels (Supplementary Fig. S7a). In this case, we noted high NFRET values, suggesting a robust interaction between HRAS-CA and RBD as compared to that between HRAS-DN and RBD (Supplementary Fig. S7b). Therefore, these HRAS mutations have contrasting effects on the interaction strength with RBD. In addition, images of HeLa cells co-expressing mVenus-HRAS + RBDCRD-mScarlet-I and mVenus-HRAS + CRAF-mScarlet-I were analyzed (Supplementary Fig. S8). High NFRET values were observed between mVenus-HRAS and RBD-mScarlet-I (Fig. 2d), which diffused across the cell. Remarkably, Fig. 2e shows that co-expression of mVenus-HRAS with RBD-Scarlet-I_NES results in a further increase in NFRET. NFRET values for positive- and negative-FRET controls and all interacting pairs are shown in Fig. 2fg. To check the effect of the varying acceptor and donor levels on FRET, the NFRET values were calculated and plotted against the acceptor-to-donor (A:D) ratio. NFRET was amplified by increasing the A:D ratio and saturated at high acceptor concentrations (Fig. 2h).

2.3. HRAS and CRAF association at the endomembranes

To validate our intermolecular FRET sensing approach, we examined HRAS-CRAF interactions at the endomembranes [44,45]. It is difficult to simultaneously observe HRAS at the cell and organelle membranes without any loss in the fluorescence signal. To overcome this challenge, we captured the z-stacks of HeLa cells expressing either mVenus-HRAS or mVenus-HRAS-DN and RBD-mScarlet-I_NES to get a better visualization of organelles (Movie S2). We found that the EGF-activated HRAS activity was most prominent at the cell membrane, moderate at the Golgi membrane, and modest at the ER membrane (Supplementary Fig. S9ab). To examine whether giantin is directly involved in the interaction with HRAS, we co-transfected the HeLa cells with pmVenus-HRAS and pmScarlet-I-giantin and analyzed the cells by seFRET. We noted the localization of HRAS and giantin at the Golgi body, as shown in the merge channel (Supplementary Fig. S9c). No significant HRAS-giantin interaction was observed at the Golgi membrane (Supplementary Fig. S9d).

2.4. Time-dependent HRAS-CRAF association in living cells

Next, time-lapsed FRET imaging was conducted. Initially, a basal FRET level was detected in the absence of EGF, and we observed a modest change in NFRET in HRAS-DN expressing HeLa cells even after the addition of EGF (Fig. 3ab, Movie S3a). In contrast, the HRAS showed a strong FRET signal in the presence of EGF (Fig. 3cd, Movie S3b). A detectable basal FRET level in the absence of EGF suggests the existence of pre-formed complexes brought about by sporadic interactions between a small fraction of HRAS and RBD molecules. Hence, this finding highlights the preexisting junctions between HRAS and CRAF, where a weak interaction occurs without the EGF inducer. To assess the photostability of mVenus and mScarlet-I, we conducted experiments where cells expressing these fluorophores were exposed to either a time-lapsed or continual illumination setting using the same laser intensity. First, cells were exposed to a 595 s-long time-lapsed illumination. In this case, we observed either a minor decrease of ~13 % in the intensity of mVenus (Supplementary Fig. 10a) or a slight reduction of ~9 % in the intensity of mScarlet-I (Supplementary Fig. 10b). These results indicate that both fluorophores are photostable at a time-lapsed illumination and can be used for long-term imaging without losing significant brightness. Second, cells were exposed to a 720-s-long continual illumination. We noted a drastic decline in the fluorescence intensity of mVenus (Supplementary Fig. S11a) and mScarlet-I (Supplementary Fig. S11b). This finding suggests that prolonged continual exposure to high-intensity light leads to a significant loss in the fluorescence intensity of these fluorophores.

2.5. Comparative analysis of HRAS-CRAF interactions using acceptor-photobleaching FRET

The conceptual formulation of abFRET is illustrated in Supplementary Fig. S12a. A typical bleaching pattern was used to bleach the acceptor (Movie S4). When the acceptor-specific high-intensity excitation light was turned on, the acceptor emission intensity decreased in a time-dependent manner (Supplementary Fig. S12b). Initially, the acceptor bleaching was performed for positive and negative FRET control-expressing cells, and images of pre- and post-bleached HeLa cells were obtained (Supplementary Fig. S13ab). Adding EGF activates EGFR and subsequent HRAS-CRAF interactions [46–48]. Images of pre- and post-bleached HeLa cells in the presence of 50 ng/ml EGF were acquired

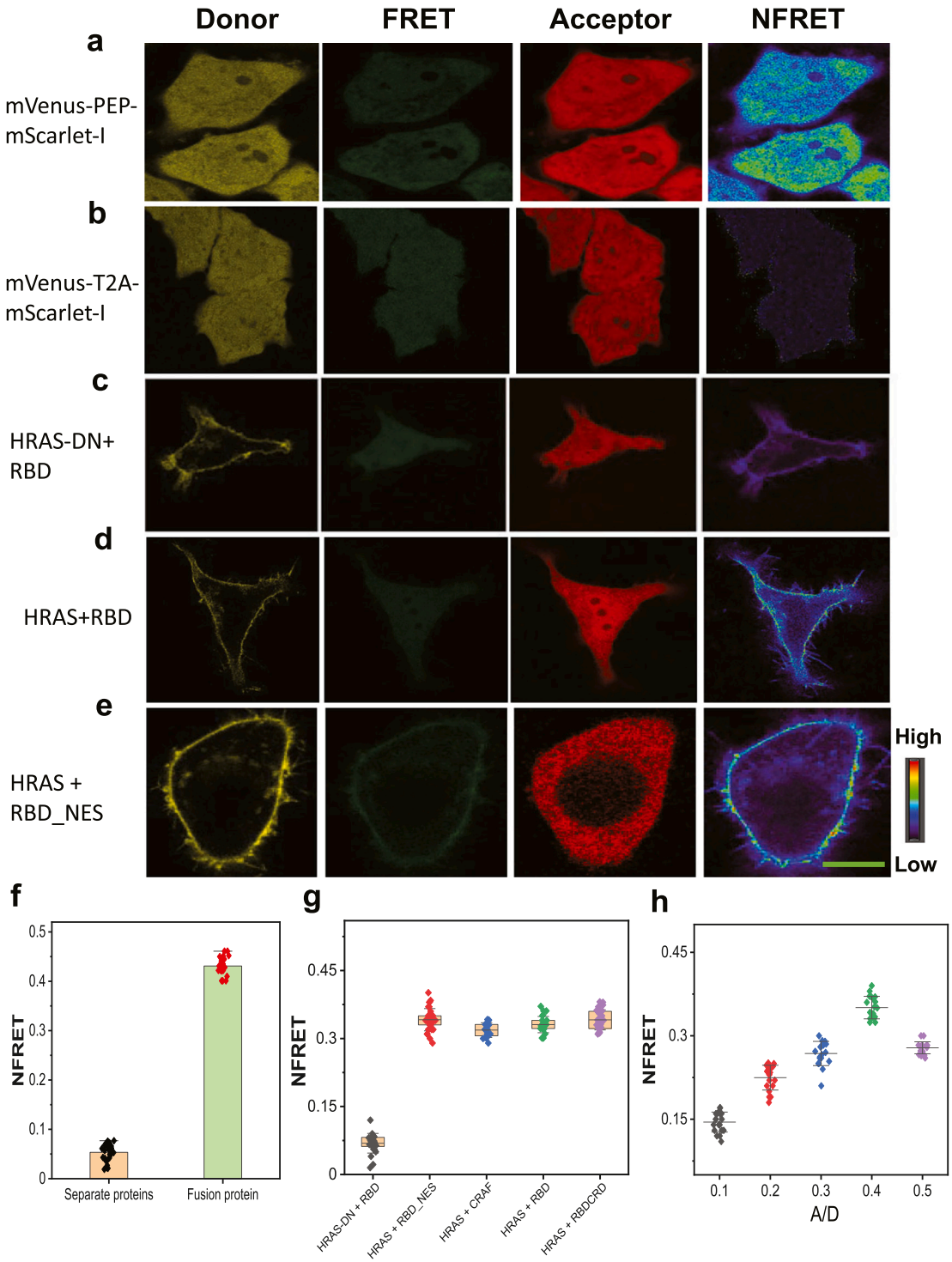

Fig. 2. Sensitized-emission FRET (seFRET) analysis for HRAS-CRAF interaction. Images of the three detection channels (donor, raw FRET, and acceptor) are shown, and the corrected NFRET image after the subtraction of spectral bleed-through [54]. (a) seFRET microscopy images of a positive FRET control. (b) seFRET microscopy images of a negative FRET control. (c) mVenus-HRAS-DN in combination with RBD-mScarlet-I. (d) mVenus-HRAS in combination with RBD-mScarlet-I. (e) mVenus-HRAS in combination with RBD-mScarlet-I_NES. (f) NFRET values for the negative- and positive-FRET controls. The numbers of cells, *n*, were 28, 23, respectively. (g) NFRET values for various binding partners (min 0 to max 0.5). From the left to right, the number of cells, *n*, were 25, 36, 16, 27, 31, respectively. (h) NFRET values for various acceptor to donor ratios of the mVenus-HRAS + RBD-mScarlet-I_NES pair. Error bars represents the standard deviation. Data are obtained using $n = 19$ cells from three independent transfections. Experiments pertinent to (c), (d), (e), (g), and (h) were obtained in the presence of 50 ng/ml EGF. Data in (f), (g), and (h) show mean ± s.d. from three independent transfections. In this study, the reported NFRET values are specifically recorded for the plasma membrane. The horizontal scale bar is 10 μm.

for co-expressed mVenus-HRAS + CRAF-mScarlet-I, mVenus-HRAS + RBD-mScarlet-I, mVenus-HRAS + RBD-mScarlet-I_NES, mVenus-HRAS-DN + RBD-mScarlet-I_NES, and mVenus-HRAS+RBDCRD-mScarlet-I (Supplementary Fig. S13c-e and Fig. S14). We found that the donor emission intensity increased in positive FRET control-expressing cells after acceptor photobleaching (Supplementary Fig. S15a).

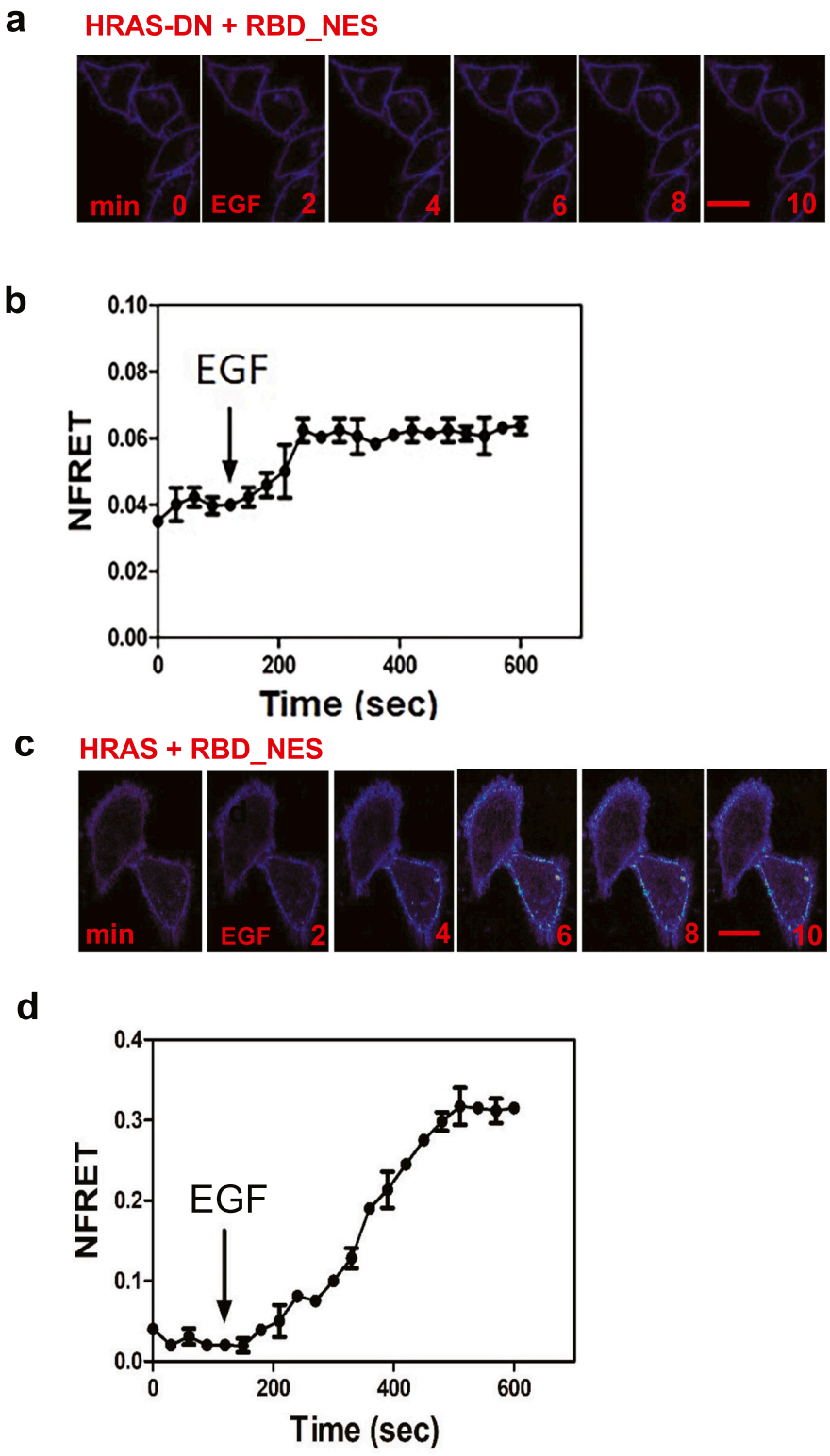

Fig. 3. Time-lapsed FRET recording in HeLa cells. (a) Real-time NFRET images of HeLa cells expressing mVenus-HRAS-DN and RBD-mScarlet-I at various time points in the presence of 50 ng/ml EGF. (b) Time dependence of NFRET values were recorded under the same experimental conditions as in (a) for 10 min. Data are obtained using $n = 7$ cells from three independent transfections. (c) NFRET images of mVenus-HRAS and RBD-mScarlet-I_NES expressing HeLa cells at various time points. Alterations in the FRET signal at the membrane were clearly noted. (d) Time dependence of NFRET values were recorded under the same experimental conditions as in (c) for 10 min. In this case, the NFRET signal increased until ~8 min, then it became saturated. Data are obtained using $n = 9$ cells from three independent transfections. The edges of the cells were selected as region of interest. NFRET varies between 0 and 0.5. In this study, the reported NFRET values are specifically recorded for the plasma membrane. The horizontal scale bar is 10 μm.

However, there was no detectable change in the donor intensity in negative FRET control-expressing cells (Supplementary Fig. S15b). mVenus-HRAS-DN and RBD-mScarlet-I co-expressing cells showed no significant difference in the post-bleaching donor intensity (Supplementary Fig. S15c). Compared with the negative FRET control, HRAS and CRAF, as well as HRAS and truncated CRAF variants, showed an increase in the post-bleaching donor emission intensity (Supplementary Fig. S16). A high FRET efficiency (36 %) was observed in the positive control because of the proximity of fluorophores, as compared to the negative control (5 %) (Supplementary Fig. S17a). Again, we found a high FRET efficiency in HeLa cells expressing truncated CRAF variants compared to the wild-type protein (Supplementary Fig. S17b). Among many formulations of FRET approaches [22], abFRET is a relatively more straightforward but underutilized qualitative method [24], necessitating fewer controls than seFRET [49]. However, to determine energy transfer efficiency, only the donor is considered, making it a less

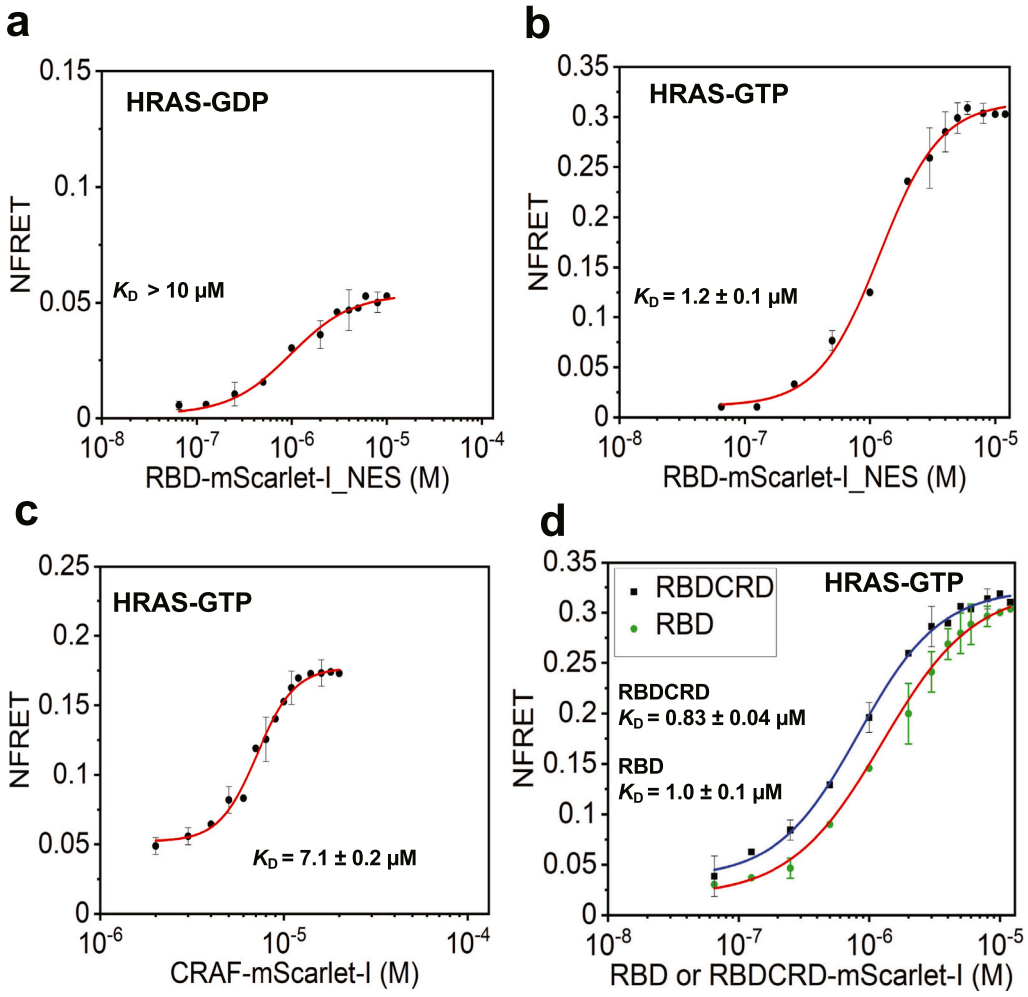

Fig. 4. *In vitro* FRET assay for the determination of the equilibrium dissociation constants, K_D. (a) mVenus-HRAS-GDP was titrated against various concentrations of RBD-mScarlet-I_NES. (b) mVenus-HRAS-GTP was titrated against various concentrations of RBD-mScarlet-I_NES. (c) mVenus-HRAS-GTP that was titrated against various concentrations of CRAF-mScarlet-I. (d) mVenus-HRAS-GTP was titrated against various concentrations of either RBD-mScarlet-I or RBDCRD-mScarlet-I. Dose responses were recorded at the donor, FRET, and acceptor channels. Finally, NFRET values were extracted and plotted against various concentrations of the acceptor, and the K_D values for different pairs were calculated. Each data point shows mean ± s.d., which were obtained from three independent replicates.

sensitive approach. In contrast, seFRET is a significantly more complex method because numerous instrumentation and post-image processing details must be considered. For example, seFRET suffers from photophysical contaminations at donor and acceptor channels. Yet, seFRET is less prone to the photodamage of fluorophores than abFRET, so it is a practical alternative for long-term imaging in living cells. Therefore, seFRET also enables repetitive FRET data acquisition, which is unachievable with abFRET. Notably, this method has the advantage of much faster rates of imaging acquisition than abFRET [50]. Hence, seFRET is more sensitive and can provide a continual time-dependent readout of energy transfer [51].

2.6. Quantitative determination of HRAS-CRAF interactions in a cell-free environment

We next measured the binding affinity between purified mVenus-HRAS and CRAF-mScarlet-I or its truncated versions using seFRET. These affinity determinations were conducted in the presence of either GDP or non-hydrolyzable GTP analog (Gpp(*NH*)p). We found weak interactions of RBD with GDP-bound HRAS compared to RBD with GTP-bound HRAS (Fig. 4ab). GTP-complexed HRAS binds with RBD-mScarlet-I_NES with high affinity, at least 10-fold higher than GDP-complexed HRAS with RBD-mScarlet-I_NES. CRAF has a lower binding affinity with HRAS than RBD (Fig. 4bc). Instead, RBDCRD has a slightly higher affinity over RBD (Fig. 4d). Notably, these binding affinities agree well with previously determined values using other existing methods (Table 1).

Table 1
Comparison of equilibrium dissociation constants, K_D, using other approaches in cell-free homogeneous solutions.

Methods	Protein pairs	K_D (μM)	References
Single-molecule fluorescence microscopy[a]	HRAS-RBD	0.35	[16]
	HRAS-CRAF	3.6	
	HRAS-DN-CRAF	~1300	
BLI[b]	KRAS-CRAF	0.41	[6]
BLI[c]	KRAS-CRAF	~1	[7]
ITC[d]	HRAS-RBD	0.45	[57]
Intermolecular seFRET[e]	HRAS-RBD	1.0 ± 0.1	This work.
	HRAS-CRAF	7.1 ± 0.2	

[a] The reaction buffer was 10 mM HEPES, 10 mM $MgCl_2$, and 0.01 % Triton X-100, pH 7.5.
[b] The reaction buffer was 20 mM HEPES, 50 mM NaCl, 20 mM $MgCl_2$, 1 mM DTT, 1 % v/v glycerol, pH 7.5.
[c] In these experiments, the BLI running buffer was 20 mM HEPES, 100 mM NaCl, 5 mM $MgCl_2$, 2 mM TCEP, 0.01 % BSA, and 0.005 % Tween-20.
[d] HRAS was used in its GTP-bound form. These experiments were conducted in 50 mM Tris-HCl, pH 7.4, 5 mM $MgCl_2$, 100 mM NaCl.
[e] This work. These FRET measurements were performed using a running buffer containing 20 mM Tris-HCl, 150 mM NaCl, 10 mM $MgCl_2$, 1 mM TCEP, pH 8. Data are reported as mean ± s.e.m.

2.7. Multiplexed imaging of the EGFR activation and HRAS-CRAF interaction in living cells

In contrast to HeLa cells, A-549 cells have a large cytoplasmic volume that can be advantageously utilized to visualize the dynamics of EGFR internalization and endocytic vesicle formation [52]. Multiplexed imaging enables simultaneous observations of two or more activities in living cells. Therefore, we asked whether we could concurrently pursue the real-time imaging of the EGFR activation and HRAS-CRAF interactions. We developed the SH2 domain (Grb2)-based biosensor to visualize and characterize the EGFR activation. A-549 cells were transfected with pmTurquoise2-SH2 and allowed to express for two days. In these experiments, we decided to use RBD instead of CRAF because of a relatively stronger interaction with HRAS (Table 1). Initially, the successful expressions of mTurquoise2-SH2, mVenus-HRAS, and RBD-mScarlet-I_NES were tested, and confocal images were acquired at the CFP, YFP, and RFP channels, respectively (Supplementary Fig. S18). To examine the EGFR activation and subsequent HRAS-RBD association, A-549 cells were EGF-activated (Fig. 5a-d). We visualized the cyan fluorescence at the edge of A-549 cells after EGF-induced activation because of the relocation of mTurquoise2-SH2 and binding to EGFR [52] (Fig. 5a). The mTurquoise2-SH2 signal was observed at the A-549 membrane about 1 min after EGF was added to the well. This initial observation confirmed the rapid EGF-induced activation and relocation of mTurquoise2-SH2 to the plasma membrane [53]. The HRAS-RBD interaction was noted about 2 min after EGF was added to the well, as evidenced by the NFRET panel (Fig. 5d). Next, we evaluated the HRAS-RBD interaction by recording the NFRET values within the same cell.

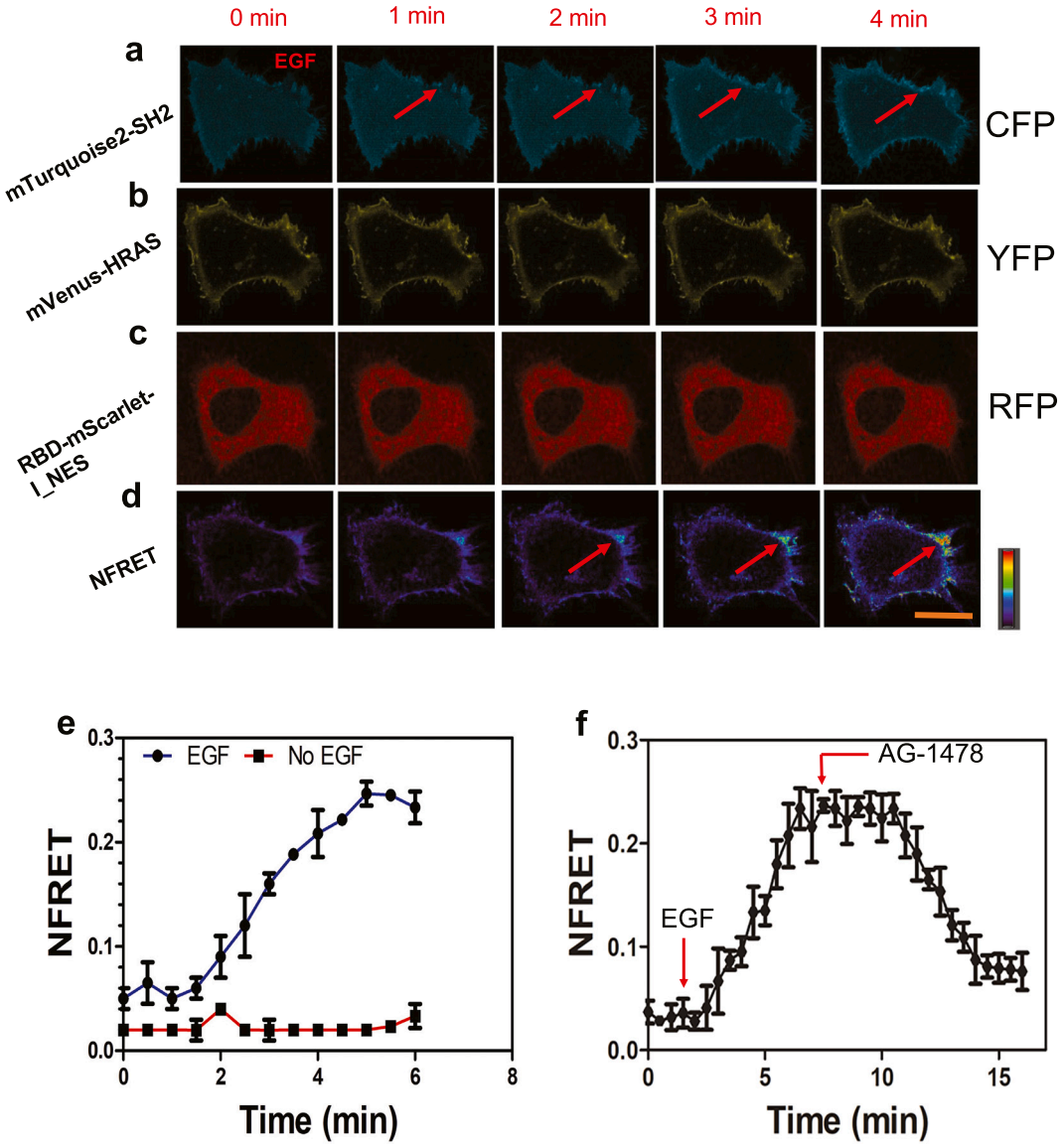

Fig. 5. Multiplexed imaging of the EGFR activation and HRAS-RBD interactions in living A-549 cells. In these experiments, we decided to use RBD instead of CRAF because of a relatively stronger interaction with HRAS (Table 1). Detection of the EGFR activation was performed in the presence of 50 ng/ml EGF. Activation of the receptor was checked by recording the images at the CFP channel. Increased cyan fluorescence was observed at the cell membrane as a function of time. HRAS-RBD interactions were detected by acquiring time-dependent FRET images. (a) mTurquoiuse2-SH2 at the CFP channel. (b) mVenus-HRAS at the YFP channel. (c) RBD-mScralet-I_NES at the RFP channel. (d) NFRET imaging. In (a) and (d), arrows indicate hot spots of the EGFR activation and HRAS-RBD interactions, respectively. In panels (a), (b), (c), and (d), the horizontal scale bar is 10 μm. (e) The NFRET values after the EGF-induced stimulation ($n = 23$). (f) Assessing the reversal of the EGF-induced stimulation. First, the EGF-induced saturation of the NFRET values was reached. Then, 250 nM AG-1478 was added to the cells after the 6-minute-long EGF incubation, and changes in the NFRET values were tracked for the following 10 min ($n = 7$). In this study, the reported NFRET values are specifically recorded for the plasma membrane. Each data point shows mean ± s.d., which were obtained from three independent replicates.

NFRET values, which were calculated according to Xia and Liu (2001) [54], increased with time and became saturated after 5 min (Fig. 5e). The fast relocation of mTurquoise2-SH2 to the plasma membrane and the rapid kinetic response of the HRAS-RBD interaction emphasize the timescale and correlation of these two processes in signal transduction. They also prove the power and utility of our biosensor for further explorations of molecular mechanisms beyond the context of EGFR signaling.

To validate that the EGF-induced association of HRAS and RBD was dependent on EGFR activation, we added AG-1478 after 6 minute-long EGF stimulation, which resulted in a gradual decrease in the NFRET signal (Supplementary Fig. 5f). AG-1478, an EGFR antagonist, functions by its binding to the ATP-binding site of the EGFR tyrosine kinase domain, preventing the receptor from autophosphorylation and triggering downstream signaling pathways that promote cell proliferation and survival. The signal was almost 90 % reversed after 9 min of AG-1478 treatment, indicating that the EGF-induced association of HRAS-RBD can be slowly reversed by inhibiting the kinase activity of EGFR. These findings suggest that this EGFR-specific inhibitor has the potential to reverse the EGF-induced stimulation of cellular signaling pathways. In a complementary experiment, we pre-incubated A-549 cells for 10 min with AG-1478. Cells were then treated with EGF, and NFRET values were recorded. Despite the EGF treatment, we found that the subsequent HRAS-RBD interaction was significantly blocked (Supplementary Fig. S19). This data demonstrates that the EGF-induced HRAS-RBD association was due to EGFR activation and suggests that AG-1478 may be a promising therapeutic compound for disrupting the HRAS-RBD interaction.

Confocal imaging of the biosensor-expressing A-549 cells showed the presence of mTurquoise2-SH2 throughout the cells (Supplementary Fig. S20a). No vesicle was observed in unstimulated A-549 cells (Supplementary Fig. S20b). Cells were treated with 50 ng/ml EGF, and images were acquired every 10 min. Following EGF-based stimulation, the SH2 domain of the Grb2 protein binds to the phosphorylated adaptor site at the cytosolic portion of EGFR [55]. We observed the formation of endocytic vesicles about 30 min after EGFR activation, which is in accord with a previously reported study (Supplementary Fig. S21) [55]. Then, the number of vesicles in A-549 cells increased with time. In this study, we selected the cells that were not saturated with the fluorescence signal (Fig. 5a and Supplementary Fig. S18, Figs. S20-S21). The NFRET value for A-549 cells was notably lower than that for HeLa cells (Fig. 2g, Fig. 3d, and Fig. 5e), despite similar expressing constructs in both cell lines. The exact reason for this discrepancy has yet to be made clear. One possible explanation is related to the expression of mTurquoise2-SH2 in A-549 cells, which may have a reversal effect on EGFR-driven signaling by sequestering phosphorylated tyrosine residues (pTyr) of EGFR and preventing the SOS recruitment (Fig. 1).

2.8. Concluding remarks

This paper describes a yellow-red pair-based intermolecular FRET method for examining HRAS-CRAF interactions in living cells and the EGFR activation through multiplexed imaging. This approach is motivated by the pressing need for novel approaches to reveal the spatiotemporal coordination of cell signaling pathways. Our method utilizes genetically encoded fluorophores with low cytotoxicity, expanded optical stability, and amplified brightness. Orthogonal affinity determinations validate these measurements in a cell-free environment. These confirmatory steps involve the same FRET pair and HRAS-CRAF interactors under GTP-activated and GDP-inactivated conditions. Finally, we measure the effect of the inhibitor on the HRAS-CRAF interaction under EGF-activated conditions. Hence, this strategy might be applied to validate the disruption of transient PPIs using critical antagonist reagents.

3. Materials and methods

3.1. Plasmids and generation of expression clones

The cDNA of HRAS was cloned in the pmVenus-C1 vector (Addgene #27794, Watertown, MA) at *BglII* and *HindIII* sites. A point mutation was introduced by Q5 site-directed mutagenesis kit (New England BioLabs, Ipswich, MA) in the HRAS to produce S17N HRAS [16], a dominant negative (DN) variant of HRAS, also named HRAS-DN. The HRAS in pmVenus-HRAS was replaced with HRAS-Q61L (HRAS-CA) at *BglII* and *HindIII* sites. The CRAF and its truncated variants, such as the RAS binding domain (RBD, residues 51-131) and RBD with cysteine-rich domain (RBDCRD, residues 51-184), were cloned in pLifeAct-mScarlet-I-N1 (Addgene #85054) at *NheI* and *BamHI* sites, in which LifeAct was replaced by our targeted gene. The nuclear-export sequence [NES, SELQNKLEELDLDSYK] [34] was genetically attached at the C terminus of the fluorophore to generate the cytosol-targeted variant of RBD-mScarlet-I. pmScarlet-I-PEP-mVenus and pmScarlet-I-T2A-mVenus were used as positive- and negative-FRET controls, respectively (Supplementary Fig. S22). Here, the sequences of PEP and T2A were SGSGLRSSDPPVAT and EGRGSLLTCGDVEENPGP, respectively [34]. pmScarlet-I-Giantin (Addgene #85048) and pmScarlet-I-KDEL (Addgene #137805) plasmids were used to visualize and identify the Golgi and ER in HeLa cells. The SH2 domain of Grb2 protein was cloned at the C terminus of pmTurquoise2 (Addgene #54842). A list of primers was used to amplify the cDNAs of the proteins mentioned above (Supplementary Table S3). All mutagenesis work was validated by DNA sequencing (Genscript, Piscataway, NJ, USA). Schematic representations of all the constructs and FRET reporters used in this study are provided in Supplementary Fig. S1 and Table S1. pmVenus-C1 was a gift from Steven Vogel (Addgene plasmid #27794). pLifeAct_mScarlet_N1, pmScarlet-I_Giantin, pmScarlet-I_KDEL, and pmTurquoise2-C1 were provided by Dorus Gadella. The corresponding Addgene plasmids are #85054, #85048, #137805, and #54842, respectively.

3.2. Cell culture and transfection

HeLa and A-549 cells were seeded on collagen-coated or non-coated six-well plates (Cellvis, Mountain View, CA) at a density of $\sim 3 \times 10^5$ cells per well and maintained in 5 % CO2 and 70 % relative humidity at 37 °C. A-549 cells were cultured in Dulbecco's modified eagle medium (DMEM-F12; ThermoFisher Scientific, Carlsbad, CA). A PCR test was used to detect mycoplasma contamination in cultures. HeLa and A-549 cells were transfected in serum-free DMEM using Fugene-HD (Promega, Madison, WI) and Lipofectamine 3000 (Invitrogen by ThermoFischer Scientific), respectively. The transfection mixture was prepared in Opti-MEM (ThermoFisher Scientific) with a transfection reagent and a plasmid DNA (1:1 ratio of donor and acceptor plasmids for co-transfection). A plasmid concentration in the range of 500–800 ng/well was used to obtain low expressors only so that the recombinant expression level was comparable to endogenous GTPase. The transfection mixture was incubated for 15–20 min at room temperature and then mixed with the cells. After 5–6 h, the transfection mixture was replaced by complete media and allowed to express the recombinant proteins. 24 h of post-transfection, the medium was replaced by DMEM for 12 h for serum starvation. Cells were washed with Dulbecco phosphate buffer saline (DPBS) and then replaced by imaging media (DMEM with 25 mM HEPES and no phenol red (ThermoFischer Scientific) before the imaging of living cells.

3.3. Live-cell imaging

The live-cell imaging was performed using a Leica SP8 confocal microscope (Leica Microsystems, Wetzlar, Germany) equipped with a white-light laser and plan apochromat objectives (63X and 100X, 1.4 NA, Leica) and controlled by LASX software (Leica). For the imaging,

living cells were maintained in an incubation chamber (Okolab USA Inc., Ambridge, PA) throughout the experiments in 5 % CO_2 at 37 °C. Initially, the imaging was performed to check the distribution of HRAS and CRAF fusion proteins, as well as single fluorescent proteins in HeLa cells. Excitation lines for mTurquoise2, mVenus, and mScarlet-I were 405, 514, and 569 nm, respectively. Spectral emissions for mTurquoise2, mVenus, and mScarlet-I were collected at 460–500 nm, 520–570 nm, and 585–670 nm, respectively. To prevent bystander FRET [56], a low-concentration of the plasmid was used. This was confirmed by fluorescence measurements of mVenus using a negative-FRET control experiment. The cells were imaged 40–48 h post-transfection. To generate the varying ratio of donor and acceptor, different amounts of the donor and acceptor plasmids were used in separate wells at the time of transfection. Living cells were first tested for positive- and negative-FRET controls (Supplementary Fig. S22). Cells were transfected separately with the acceptor and donor-only plasmids to measure the direct excitation of the acceptor at the donor excitation and the emission of the donor into the FRET channel, respectively. Cells were transfected with pmScarlet-I-PEP-mVenus and pmScarlet-I-T2A-mVenus. 24 h post-transfection, the cells were imaged in the lambda-scanning mode of the microscope. Positive- and negative-FRET controls expressed in HeLa cells were excited by 510 nm, and the emission was recorded at 520–650 nm with a step-size of 3 nm for both samples. To check the photostability of mVenus and mScarlet-I, HeLa cells were transfected with pmVenus and pmScarlet-I, and imaging was performed under time-lapsed and continuous illumination at a 2 % laser intensity. The excitation and emission lines were set up as indicated above.

3.4. Sensitized-emission FRET microscopy (seFRET) for determining HRAS-CRAF interactions

HeLa cells were transfected with the donor only, the acceptor only, and the donor plus acceptor fluorophores containing plasmids. They were stimulated by applying 50 ng/ml EGF. The seFRET imaging was conducted at 63× magnification with 50 % neutral density filters. As mentioned earlier, the cells were illuminated with a specific laser, and the emission was captured on a cooled charge-coupled device (CCD) camera. The emission was collected using HyD detectors for mVenus, a yellow fluorescent protein (YFP; 500 ms excitation), mScarlet-I, a red fluorescent protein (RFP; 500 ms), and seFRET (sensitized RFP emission; 514 nm excitation filter, 500 ms, 585–670 nm spectral emission filter). The donor bleed-through and acceptor crosstalk were corrected by the donor-only and the acceptor-only expressing cells. The normalized sensitized-emission FRET (NFRET) efficiency effectively compares the FRET-positive and FRET-negative samples, providing more tractable FRET measurements with a reduced standard error (<5 %). A pseudo color was given to every image, and the background was subtracted. NFRET was calculated according to Xia and Liu (2001) [54]:

$$\mathrm{NFRET} = \frac{I_{\mathrm{FRET}} - \alpha I_{\mathrm{mScarlet-I}} - \beta I_{\mathrm{mVenus}}}{\sqrt{I_{\mathrm{mScarlet-I}} I_{\mathrm{mVenus}}}} \quad (1)$$

Here, $I_{\mathrm{mScarlet\text{-}I}}$ is the intensity of the acceptor, and I_{mVenus} denotes the intensity of the donor. I_{FRET} is the FRET intensity. α indicates the acceptor spectral bleed-through. β is the donor spectral bleed-through. NFRET is based on the measurement of three distinct combinations of excitation wavelengths and spectral emission filters: (i) a donor-detection channel combining a donor-specific excitation with a donor-specific emission filter, (ii) a raw FRET channel employing a donor-specific excitation and an acceptor-specific emission filter, and (iii) an acceptor channel using an acceptor-specific excitation and an acceptor-specific emission filter. For the organelle visualization, z-stacks were captured with a 5.4 μm-thick slice. Each section was 0.415 μm, which started at −12.35 μm and ended at −17.75 μm.

3.5. Affinity measurements in a cell-free environment

29,39-O-N methyl anthraniloyl–GppNHp (Gpp(*NH*)p), a non-hydrolyzable GTP, and GDP were added to purified mVenus-HRAS and mVenus-HRAS-DN. Samples were incubated in the presence of 15 mM ethylene diamine tetra acetic acid (EDTA) for 30 min at 37 °C, followed by adding 10 mM $MgCl_2$ to the reaction. The excess Gpp(*NH*)p and GDP were removed with a desalting column. Various concentrations of the purified CRAF-mScarlet-I, or its truncated versions, were mixed and incubated at room temperature for 30 min. FRET emissions were measured using a Spectramax i3 multimodal automated plate reader (Molecular Devices, San Jose, CA). This instrument was equipped with monochromators that allow the individual optimization of wavelengths for the excitation and emission using photomultiplier tubes (PMT). Excitations of mVenus and mScarlet-I were performed at 500 and 570 nm, respectively. The FRET emission was read at 595 nm. NFRET values were determined using the acceptor crosstalk and donor bleed-through contributions. The FRET signal between mVenus and mScarlet-I was quantified with a sensitized emission of the acceptor. A graph was plotted between the NFRET value and the ligand concentration. The dissociation constant, K_D, was calculated using the following equation:

$$\mathrm{NFRET} = \frac{\mathrm{FRET}_{\max}[\mathrm{L}] + \mathrm{NS}[\mathrm{L}] + \mathrm{B}[\mathrm{L}]}{\mathrm{K_D} + [\mathrm{L}]} \quad (2)$$

A single-site binding model determined K_D values by fitting the steady-state response against the acceptor concentration. Here, NFRET and FRETmax are the normalized seFRET signal and the maximum FRET value at saturation, respectively. [L], NS, and B, denote the ligand concentration, the FRET signal due to non-specific binding, and the FRET signal due to non-specific binding without the acceptor, respectively.

3.6. Multiplexed imaging of the EGFR activity and HRAS-CRAF interactions

To visualize the EGFR activity in living cells, we selected A-549 lung cancer cells, which provide an opportunity to monitor vesicle formation post-EGF stimulation. We constructed a biosensor using the SH2 domain of Grb_2 protein genetically fused at the C terminus of mTurquoise2, generating mTurquoise2-SH2. A-549 cells were seeded in a six-well glass bottom plate and grown in advanced DMEM-F12 supplemented with 10 % fetal bovine serum (FBS; ThermoFisher Scientific) and 1 % penicillin-streptomycin in 5 % CO_2 at 37 °C. Cells were transfected at 60–70 % confluency by pmTurquoise2-SH2 using Lipofectamine 3000 (Invitrogen) and grown for an additional 40–48 h. Cells were washed with warm DPBS three times, and the medium was exchanged with DMEM for overnight serum starvation. Finally, cells were washed with DPBS, and the imaging medium was added. For multiplexed imaging, A-549 cells were co-transfected with three plasmids, namely, pmTurquoise2-SH2, pmVenus-HRAS, and pRBD-mScarlet-I_NES, and allowed to express the recombinant proteins for 40–48 h. Crosstalk and bleed-through contributions were corrected, and final NFRET images were generated.

This file includes the following items: Supplementary methods; list of constructs used in this study; characterization of positive- and negative-control FRET constructs; localization and distribution of HRAS and CRAF in living cells; sensitized-emission FRET of HRAS-CRAF interactions; acceptor-photobleaching FRET of HRAS-CRAF interactions; characterization of EGFR biosensor and time-dependent EGFR activation; list of primers used in this work; supplementary references.Supplementary data to this article can be found online at doi:https://doi.org/10.1016/j.bbamem.2023.184173.

CRediT authorship contribution statement

M.A. and L.M. designed research. M.A. performed research, analyzed data, and worked on data interpretations. M.A. and L.M. wrote the paper.

Declaration of competing interest

The authors declare that they have no known competing financial interests or personal relationships that could have appeared to influence the work reported in this paper.

Data availability

Data will be made available on request.

Acknowledgments

Authors are grateful to Leszek Kotula (SUNY Upstate Medical University, Syracuse, NY) for his help in the very early stages of this project and Tae-Young Yoon (Yonsei University, Seoul, South Korea) for providing plasmids containing genes that encode HRAS and CRAF proteins. We are grateful to Joshuo Wang (Center of Excellence for Advanced Light Microscopy) at SUNY Upstate Medical University (Syracuse, NY) for technical assistance with confocal microscopy. This study was supported by the U.S. National Institutes of Health, grants R01 GM088403 (to L.M.) and R01 EB033412 (to L.M.).

References

[1] T. Tomida, Visualization of the spatial and temporal dynamics of MAPK signaling using fluorescence imaging techniques, J. Physiol. Sci. 65 (2015) 37–49.
[2] S. Lu, H. Jang, S. Muratcioglu, A. Gursoy, O. Keskin, R. Nussinov, J. Zhang, Ras conformational ensembles, allostery, and signaling, Chem. Rev. 116 (2016) 6607–6665.
[3] A.C. Nelson, T.J. Turbyville, S. Dharmaiah, M. Rigby, R. Yang, T.Y. Wang, J. Columbus, R. Stephens, T. Taylor, D. Sciacca, G. Onsongo, A. Sarver, S. Subramanian, D.V. Nissley, D.K. Simanshu, E. Lou, RAS internal tandem duplication disrupts GTPase-activating protein (GAP) binding to activate oncogenic signaling, J. Biol. Chem. 295 (2020) 9335–9348.
[4] R. Barbosa, L.A. Acevedo, R. Marmorstein, The MEK/ERK network as a therapeutic target in human cancer, Mol. Cancer Res. 19 (2021) 361–374.
[5] S.K. Fetics, H. Guterres, B.M. Kearney, G. Buhrman, B. Ma, R. Nussinov, C. Mattos, Allosteric effects of the oncogenic RasQ61L mutant on Raf-RBD, Structure 23 (2015) 505–516.
[6] M.J. Kauke, M.W. Traxlmayr, J.A. Parker, J.D. Kiefer, R. Knihtila, J. McGee, G. Verdine, C. Mattos, K.D. Wittrup, An engineered protein antagonist of K-Ras/B-Raf interaction, Sci. Rep. 7 (2017) 5831.
[7] C.W. Johnson, H.S. Seo, E.M. Terrell, M.H. Yang, F. KleinJan, T. Gebregiworgis, G. M.C. Gasmi-Seabrook, E.A. Geffken, J. Lakhani, K. Song, P. Bashyal, O. Popow, J. A. Paulo, A. Liu, C. Mattos, C.B. Marshall, M. Ikura, D.K. Morrison, S. Dhe-Paganon, K.M. Haigis, Regulation of GTPase function by autophosphorylation, Mol. Cell 82 (2022) 950–968.e914.
[8] C. Guzmán, M. Šolman, A. Ligabue, O. Blaževitš, D.M. Andrade, L. Reymond, C. Eggeling, D. Abankwa, The efficacy of Raf kinase recruitment to the GTPase H-ras depends on H-ras membrane conformer-specific nanoclustering, J. Biol. Chem. 289 (2014) 9519–9533.
[9] T. Travers, C.A. López, C. Agamasu, J.J. Hettige, S. Messing, A.E. García, A. G. Stephen, S. Gnanakaran, Anionic lipids impact RAS-binding site accessibility and membrane binding affinity of CRAF RBD-CRD, Biophys. J. 119 (2020) 525–538.
[10] R. Nussinov, C.J. Tsai, H. Jang, Ras assemblies and signaling at the membrane, Curr. Opin. Struct. Biol. 62 (2020) 140–148.
[11] E.M. Terrell, D.E. Durrant, D.A. Ritt, N.E. Sealover, E. Sheffels, R. Spencer-Smith, D. Esposito, Y. Zhou, J.F. Hancock, R.L. Kortum, D.K. Morrison, Distinct binding preferences between Ras and Raf family members and the impact on oncogenic Ras signaling, Mol. Cell 76 (2019) 872–884.e875.
[12] H. De Keersmaecker, R. Camacho, D.M. Rantasa, E. Fron, I.H. Uji, H. Mizuno, S. Rocha, Mapping transient protein interactions at the nanoscale in living mammalian cells, ACS Nano 12 (2018) 9842–9854.
[13] A.K. Thakur, L. Movileanu, Real-time measurement of protein-protein interactions at single-molecule resolution using a biological nanopore, Nature Biotechnol. 37 (2019) 96–101.
[14] A.K. Thakur, L. Movileanu, Single-molecule protein detection in a biofluid using a quantitative nanopore sensor, ACS Sens. 4 (2019) 2320–2326.
[15] C. Kiel, D. Filchtinski, M. Spoerner, G. Schreiber, H.R. Kalbitzer, C. Herrmann, Improved binding of raf to Ras.GDP is correlated with biological activity, J. Biol. Chem. 284 (2009) 31893–31902.
[16] J. Yoo, T.S. Lee, B. Choi, M.J. Shon, T.Y. Yoon, Observing extremely weak protein-protein interactions with conventional single-molecule fluorescence microscopy, J. Am. Chem. Soc. 138 (2016) 14238–14241.
[17] C.E. Quevedo, A. Cruz-Migoni, N. Bery, A. Miller, T. Tanaka, D. Petch, C.J. R. Bataille, L.Y.W. Lee, P.S. Fallon, H. Tulmin, M.T. Ehebauer, N. Fernandez-Fuentes, A.J. Russell, S.B. Carr, S.E.V. Phillips, T.H. Rabbitts, Small molecule inhibitors of RAS-effector protein interactions derived using an intracellular antibody fragment, Nat. Commun. 9 (2018) 3169.
[18] L. Gremer, A. De Luca, T. Merbitz-Zahradnik, B. Dallapiccola, S. Morlot, M. Tartaglia, K. Kutsche, M.R. Ahmadian, G. Rosenberger, Duplication of Glu37 in the switch I region of HRAS impairs effector/GAP binding and underlies Costello syndrome by promoting enhanced growth factor-dependent MAPK and AKT activation, Hum. Mol. Genet. 19 (2010) 790–802.
[19] H. Kobayashi, L.P. Picard, A.M. Schönegge, M. Bouvier, Bioluminescence resonance energy transfer-based imaging of protein-protein interactions in living cells, Nat. Protoc. 14 (2019) 1084–1107.
[20] S. Voss, D.M. Krüger, O. Koch, Y.W. Wu, Spatiotemporal imaging of small GTPases activity in live cells, Proc. Natl. Acad. Sci. U. S. A. 113 (2016) 14348–14353.
[21] J. Kim, S. Lee, K. Jung, W.C. Oh, N. Kim, S. Son, Y. Jo, H.B. Kwon, W.D. Heo, Intensiometric biosensors visualize the activity of multiple small GTPases in vivo, Nat. Commun. 10 (2019) 211.
[22] W.R. Algar, N. Hildebrandt, S.S. Vogel, I.L. Medintz, FRET as a biomolecular research tool - understanding its potential while avoiding pitfalls, Nat. Methods 16 (2019) 815–829.
[23] E. Lerner, A. Barth, J. Hendrix, B. Ambrose, V. Birkedal, S.C. Blanchard, R. Börner, H. Sung Chung, T. Cordes, T.D. Craggs, A.A. Deniz, J. Diao, J. Fei, R.L. Gonzalez, I. V. Gopich, T. Ha, C.A. Hanke, G. Haran, N.S. Hatzakis, S. Hohng, S.C. Hong, T. Hugel, A. Ingargiola, C. Joo, A.N. Kapanidis, H.D. Kim, T. Laurence, N.K. Lee, T. H. Lee, E.A. Lemke, E. Margeat, J. Michaelis, X. Michalet, S. Myong, D. Nettels, T. O. Peulen, E. Ploetz, Y. Razvag, N.C. Robb, B. Schuler, H. Soleimaninejad, C. Tang, R. Vafabakhsh, D.C. Lamb, C.A. Seidel, S. Weiss, FRET-based dynamic structural biology: challenges, perspectives and an appeal for open-science practices, Elife vol. 10 (2021).
[24] K.H. Rainey, G.H. Patterson, Photoswitching FRET to monitor protein-protein interactions, Proc. Natl. Acad. Sci. U. S. A. 116 (2019) 864–873.
[25] B. Hochreiter, M. Kunze, B. Moser, J.A. Schmid, Advanced FRET normalization allows quantitative analysis of protein interactions including stoichiometries and relative affinities in living cells, Sci. Rep. 9 (2019) 8233.
[26] D.R. Singh, M.M. Mohammad, S. Patowary, J.A. Oliver, L. Movileanu, V. Raicu, Determination of the quaternary structure of a bacterial ATP-Binding Cassette (ABC) transporter in living cells, Integr. Biol. 5 (2013) 312–323.
[27] J.L. Vinkenborg, T.J. Nicolson, E.A. Bellomo, M.S. Koay, G.A. Rutter, M. Merkx, Genetically encoded FRET sensors to monitor intracellular Zn2+ homeostasis, Nat. Methods 6 (2009) 737–740.
[28] X. Zhou, T.L. Clister, P.R. Lowry, M.M. Seldin, G.W. Wong, J. Zhang, Dynamic visualization of mTORC1 activity in living cells, Cell Rep. 10 (2015) 1767–1777.
[29] E.A. Rodriguez, R.E. Campbell, J.Y. Lin, M.Z. Lin, A. Miyawaki, A.E. Palmer, X. Shu, J. Zhang, R.Y. Tsien, The growing and glowing toolbox of fluorescent and photoactive proteins, Trends Biochem. Sci. 42 (2017) 111–129.
[30] Z.H. Wei, H. Chen, C. Zhang, B.C. Ye, FRET-based system for probing protein-protein interactions between σR and RsrA from Streptomyces coelicolor in response to the redox environment, PLoS One 9 (2014), e92330.
[31] T. Nagai, K. Ibata, E.S. Park, M. Kubota, K. Mikoshiba, A. Miyawaki, A variant of yellow fluorescent protein with fast and efficient maturation for cell-biological applications, Nat. Biotechnol. 20 (2002) 87–90.
[32] G.J. Kremers, J. Goedhart, E.B. van Munster, T.W. Gadella Jr., Cyan and yellow super fluorescent proteins with improved brightness, protein folding, and FRET Förster radius, Biochemistry 45 (2006) 6570–6580.
[33] D.S. Bindels, L. Haarbosch, L. van Weeren, M. Postma, K.E. Wiese, M. Mastop, S. Aumonier, G. Gotthard, A. Royant, M.A. Hink, T.W. Gadella Jr., mScarlet: a bright monomeric red fluorescent protein for cellular imaging, Nat. Methods 14 (2017) 53–56.
[34] J. Goedhart, D. von Stetten, M. Noirclerc-Savoye, M. Lelimousin, L. Joosen, M. A. Hink, L. van Weeren, T.W.J. Gadella, A. Royant, Structure-guided evolution of cyan fluorescent proteins towards a quantum yield of 93%, Nat. Commun. 3 (2012) 751.
[35] M.R. Packer, J.A. Parker, J.K. Chung, Z. Li, Y.K. Lee, T. Cookis, H. Guterres, S. Alvarez, M.A. Hossain, D.P. Donnelly, J.N. Agar, L. Makowski, M. Buck, J. T. Groves, C. Mattos, Raf promotes dimerization of the Ras G-domain with increased allosteric connections, Proc. Natl. Acad. Sci. U. S. A. 118 (2021).
[36] T.H. Tran, A.H. Chan, L.C. Young, L. Bindu, C. Neale, S. Messing, S. Dharmaiah, T. Taylor, J.P. Denson, D. Esposito, D.V. Nissley, A.G. Stephen, F. McCormick, D. K. Simanshu, KRAS interaction with RAF1 RAS-binding domain and cysteine-rich domain provides insights into RAS-mediated RAF activation, Nat. Commun. 12 (2021) 1176.
[37] S. Surve, S.C. Watkins, A. Sorkin, EGFR-RAS-MAPK signaling is confined to the plasma membrane and associated endorecycling protrusions, J. Cell Biol. 220 (2021).
[38] D.J.M. Bergen, N.L. Stevenson, R.E.H. Skinner, D.J. Stephens, C.L. Hammond, The Golgi matrix protein giantin is required for normal cilia function in zebrafish, Biol. Open 6 (2017) 1180–1189.
[39] S. Yoshimura, A. Yamamoto, Y. Misumi, M. Sohda, F.A. Barr, G. Fujii, A. Shakoori, H. Ohno, K. Mihara, N. Nakamura, Dynamics of Golgi matrix proteins after the blockage of ER to Golgi transport, J. Biochem. 135 (2004) 201–216.
[40] D.A. Ritt, M.T. Abreu-Blanco, L. Bindu, D.E. Durrant, M. Zhou, S.I. Specht, A. G. Stephen, M. Holderfield, D.K. Morrison, Inhibition of Ras/Raf/MEK/ERK pathway signaling by a stress-induced phospho-regulatory circuit, Mol. Cell 64 (2016) 875–887.
[41] J.C. Hunter, A. Manandhar, M.A. Carrasco, D. Gurbani, S. Gondi, K.D. Westover, Biochemical and structural analysis of common cancer-associated KRAS mutations, Mol. Cancer Res. 13 (2015) 1325–1335.

[42] S.E. Acuner, F. Sumbul, H. Torun, T. Haliloglu, Oncogenic mutations on Rac1 affect global intrinsic dynamics underlying GTP and PAK1 binding, Biophys. J. 120 (2021) 866–876.
[43] G.A. Hobbs, C.J. Der, K.L. Rossman, RAS isoforms and mutations in cancer at a glance, J. Cell Sci. 129 (2016) 1287–1292.
[44] V.K. Chiu, T. Bivona, A. Hach, J.B. Sajous, J. Silletti, H. Wiener, R.L. Johnson 2nd, A.D. Cox, M.R. Philips, Ras signalling on the endoplasmic reticulum and the Golgi, Nat. Cell Biol. 4 (2002) 343–350.
[45] I.A. Prior, J.F. Hancock, Ras trafficking, localization and compartmentalized signalling, Semin. Cell Dev. Biol. 23 (2012) 145–153.
[46] K. Hibino, T.M. Watanabe, J. Kozuka, A.H. Iwane, T. Okada, T. Kataoka, T. Yanagida, Y. Sako, Single- and multiple-molecule dynamics of the signaling from H-Ras to cRaf-1 visualized on the plasma membrane of living cells, Chemphyschem 4 (2003) 748–753.
[47] K. Hibino, T. Shibata, T. Yanagida, Y. Sako, A RasGTP-induced conformational change in C-RAF is essential for accurate molecular recognition, Biophys. J. 97 (2009) 1277–1287.
[48] K. Hibino, T. Shibata, T. Yanagida, Y. Sako, Activation kinetics of RAF protein in the ternary complex of RAF, RAS-GTP, and kinase on the plasma membrane of living cells: single-molecule imaging analysis, J. Biol. Chem. 286 (2011) 36460–36468.
[49] J.A. Brzostowski, T. Meckel, J. Hong, A. Chen, T. Jin, Imaging protein-protein interactions by Förster resonance energy transfer (FRET) microscopy in live cells, Curr. Protoc. Protein. Sci. Chapter 19 (2009) (19.15.11-19.15.12).
[50] R. Eckenstaler, R.A. Benndorf, A combined acceptor photobleaching and donor fluorescence lifetime imaging microscopy approach to analyze multi-protein interactions in living cells, Front. Mol. Biosci. 8 (2021), 635548.
[51] S.M. Müller, H. Galliardt, J. Schneider, B.G. Barisas, T. Seidel, Quantification of Förster resonance energy transfer by monitoring sensitized emission in living plant cells, Front. Plant Sci. 4 (2013) 413.
[52] A. Tomas, C.E. Futter, E.R. Eden, EGF receptor trafficking: consequences for signaling and cancer, Trends Cell Biol. 24 (2014) 26–34.
[53] C. Hu, C.A. Leche 2nd, A. Kiyatkin, Z. Yu, S.E. Stayrook, K.M. Ferguson, M. A. Lemmon, Glioblastoma mutations alter EGFR dimer structure to prevent ligand bias, Nature 602 (2022) 518–522.
[54] Z. Xia, Y. Liu, Reliable and global measurement of fluorescence resonance energy transfer using fluorescence microscopes, Biophys. J. 81 (2001) 2395–2402.
[55] D. Lee, J. Lim, K.C. Woo, K.T. Kim, Piperonylic acid stimulates keratinocyte growth and survival by activating epidermal growth factor receptor (EGFR), Sci. Rep. 8 (2018) 162.
[56] A.H. Clayton, A. Chattopadhyay, Taking care of bystander FRET in a crowded cell membrane environment, Biophys. J. 106 (2014) 1227–1228.
[57] M.G. Rudolph, T. Linnemann, P. Grunewald, A. Wittinghofer, I.R. Vetter, C. Herrmann, Thermodynamics of Ras/effector and Cdc42/effector interactions probed by isothermal titration calorimetry, J. Biol. Chem. 276 (2001) 23914–23921.